

CLOSED-FORM SOLUTION TO THE SCATTERING OF A SKEW STRIP FIELD BY METALLIC PIN IN A SLAB

C. A. Valagiannopoulos

School of Electrical and Computer Engineering
National Technical University of Athens
GR 157–73. Zografou, Athens, Greece

Abstract—A tiny metallic cylinder placed into a planar dielectric waveguide scatters the field developed by a current-carrying skew strip centralized at the middle of the slab. Due to the small size of the scatterer, the induced surface current is taken independent of the azimuthal angle. The Green's function of the problem is expressed in closed form and it is inserted to the scattering integral after the polar equation of the strip has been determined. The behavior of near-field quantities in the slab, with respect to geometrical and material parameters, is observed and examined.

1. INTRODUCTION

Optical waveguiding structures utilizing planar dielectric slabs are extensively used and analyzed for many years. The treatment of the original problem is contained in [1], while a modified version is investigated in [2] where the cut-off wavenumbers and the resonant frequencies are derived. An interesting study concerning dielectric loadings in parallel-plate waveguides is presented in [3]. The formal solution is obtained through Wiener-Hopf equations and the asymptotic form via approximate evaluation of integrals and series. Moreover, a two-dimensional magneto-dielectric grating slab is examined in [4] where the transmission and reflection coefficients of this two-port system are deduced with use of the generalized scattering matrix method. In [5] the authors apply the analytical continuity principle with mode matching technique to compute the reflection and transmission coefficients for a waveguide terminated in free space with a tilted facet, whereas in [6] the slab is constructed by a uniaxially anisotropic dispersive metamaterial. In [7] a study concerning the

linear mode inside a left-handed dielectric waveguide is provided, and in [8] the planar slab is illuminated by a plane wave.

Metallic components are commonly incorporated into dielectric slabs to improve the performance and the operation of the devices. In [9], the authors inquire into the scattering of guided waves inside the dielectric waveguide by a metallic cylinder. The S-matrix elements and the transfer function of such a filter are calculated. Furthermore, the effect of periodic metallizations, placed at the surface of the slab, on the propagated waves has been investigated [10]. The array of patches is considered as a perturbation of the initial structure and the resonances of this absorbing screen are studied. Also in [11], a parasitic patch is placed on the dielectric of a resonator antenna and a rigorous formulation is developed. The input impedance and the radiation features are determined by implementing an efficient computational technique. Finally, in [12] a rectangular metallization assists the radiation of a multi-layered sphere.

Dielectric waveguides as the aforementioned ones can be excited by a variety of sources such as monopoles, dipoles or plane waves. Strips flown by arbitrary current are employed as a convenient alternative source. In [13], a sensor device for an electromagnetic tomography system is fed by numerous strips. Owing to the independent control of them, three different excitation protocols can be generated. In general, slot antennas are usually excited by microstrip feed lines [14]. Also, in [15] a normal strip of axial current produces the incident field to an anisotropic cylinder with full permittivity matrix. The distribution of the current can be defined by any smooth function. In [16] a triangular microstrip field for ultra wideband applications is analyzed and in [17] a rectangular dielectric resonator is also excited by a current-carrying strip.

In this work we suppose a small metallic cylinder (pin) into the slab, while the whole structure is excited by a skew strip of constant current embedded in the waveguide. In such a problem, the issue of scattering by inhomogeneities occurred in dielectric slabs is combined with a nontrivial excitation source. Due to the tiny size of the metallic pin, closed-form solution is obtained and therefore the structure is worth to be investigated. The Green's function of the examined problem is comprised of three terms: (a) the singular free-space one, (b) the primary one expressing the effect of the slab in the absence of the pin and (c) the secondary one indicating the influence of the cylindrical scatterer itself. The first term is well-known and represents a cylindrical wave. The second term is written as a rapidly converging spectral integral. The third term is computed by supposing azimuthally independent current around the cylinder because of its

small radius. The total field is written as a line integral on the strip which can be numerically evaluated. The polar equation of the strip is necessary to formulate such an integral and thus it is rigorously determined. The variations of the distributed energy with respect to the slab's material and thickness, to the length and the inclination of the strip's line and the spatial parameters are presented and discussed.

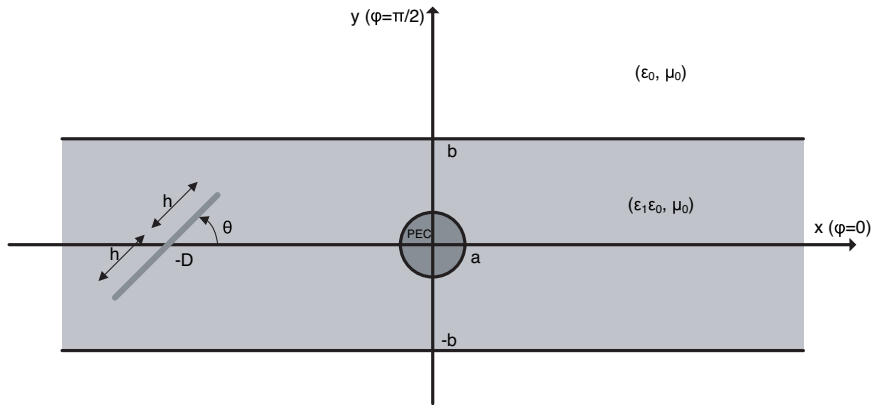


Figure 1. The physical configuration of the analyzed device. A small metallic pin inside the dielectric slab scatters the field emanating from a skew strip flown by constant electric current.

2. STATEMENT OF THE PROBLEM

We consider an infinite dielectric slab of thickness $2b$ constructed by lossless and magnetically inert material with relative permittivity $\epsilon_1 > 1$. The background medium is vacuum with wavenumber $k_0 = 2\pi/\lambda_0$ and intrinsic impedance $\zeta_0 = 120\pi \Omega$. The symbol λ_0 is used for the free space wavelength, whereas the wavenumber for the slab's material is denoted by $k_1 = k_0\sqrt{\epsilon_1}$. A two-dimensional metallic cylinder with infinitesimal radius a ($a \ll \min(b, \lambda_0)$) is located in the middle of the dielectric waveguide. The physical configuration of the device is depicted in Fig. 1, where the cartesian (x, y, z) and the equivalent cylindrical (ρ, ϕ, z) coordinate systems are also defined (their common origin coincides with the center of the cylinder). The structure is excited by a strip posed into the slab, infinite towards the z axis, flown by constant and z -polarized surface electric current I (expressed in A/m). The length of the strip, which is placed relatively far from the pin, equals to $2h$ ($h < b$), while its center is the point $(x = -D, y = 0)$

in cartesian coordinates. The line of the strip forms an arbitrary angle $\theta \in (0, \pi)$ with the x axis.

It should be stressed that both the excitation current and the shape of the device are invariant along the z axis. Given the fact that the source is of electric type, the single component of the electric field is parallel to z axis. The purpose of this work is to provide a closed-form solution to the described problem, giving the physical insight on the system under investigation. This is possible if one avoids implementing numerical techniques (including method of moments [18]) during the analysis of the problem. We wish to use analytical tools in the most part of the derivation of the solution and observe its dependencies on geometrical and material parameters. A harmonic time of $\exp(+j2\pi ft)$ form is adopted and suppressed.

3. PRIMARY GREEN'S FUNCTION DERIVATION

In this section, we are aiming at the determination of the Green's function of the reduced problem, formulated in the absence of the perfectly conducting (PEC) cylinder. The required quantity equals to the singular excitation plus the so-called "primary" Green's function. We will perform the derivation of the axial electric field developed by a filamentary two-dimensional electric dipole located inside the dielectric waveguide, across the axis ($x = X$, $y = Y$) or alternatively ($\rho = P$, $\phi = \Phi$) in cylindrical coordinates. Each of the alternative positions of the dipole represents a different point of the strip's line. The magnitude of the excitation current equals $j/(k_0\zeta_0)$ (expressed in A) which is dictated by the definition of the Green's function and the free space permeability of the slab's material [19]. The notations $G_{1,prim}$, $G_{0,prim}^U$, $G_{0,prim}^L$ correspond to the field inside the slab, in the upper vacuum half space and in the lower half one respectively. The field of the singular source is given by [20]:

$$\begin{aligned} G_{1,sing}(x, y, X, Y) &= -\frac{j}{4} H_0^{(2)} \left(k_1 \sqrt{(x-X)^2 + (y-Y)^2} \right) \\ &= \frac{1}{4\pi} \int_{-\infty}^{+\infty} e^{-js(x-X)} \frac{\exp(-g_1|y-Y|)}{g_1} ds \quad (1) \end{aligned}$$

where $H_u^{(2)}$ is the Hankel function of second type and u -th order. The symbols $g_i = g_i(s) = \sqrt{s^2 - k_i^2}$ with $i = 0, 1$ stand for the radiation functions in each area having positive (or zero) real and imaginary parts $\Re[g_i], \Im[g_i] \geq 0$.

The suitable boundary conditions indicating the continuity of the tangential electromagnetic fields across the separating planes $y = \pm b$

are given below.

$$G_{1,sing}(x, \pm b, X, Y) + G_{1,prim}(x, \pm b, X, Y) = G_{0,prim}^{U/L}(x, \pm b, X, Y) \quad (2)$$

$$\frac{\partial G_{1,sing}(x, \pm b, X, Y)}{\partial y} + \frac{\partial G_{1,prim}(x, \pm b, X, Y)}{\partial y} = \frac{\partial G_{0,prim}^{U/L}(x, \pm b, X, Y)}{\partial y} \quad (3)$$

The normal derivatives are continuous because of the magnetically inert dielectric material of the slab. By using the related integral representations for the solutions of the homogeneous cartesian Helmholtz equation (similar to the second line of (1)) and by taking into account the Sommerfeld's radiation condition, the expressions (2), (3) yield to a 4×4 linear system with respect to the unknown coefficient integrands. Once it is solved, the form of the primary Green's function for observation points inside the slab is explicitly specified:

$$G_{1,prim}(x, y, X, Y) = \frac{1}{4\pi} \int_{-\infty}^{+\infty} e^{-g_1 b} \frac{g_1 - g_0}{g_1} e^{-js(x-X)} \cdot \frac{e^{g_1 b}(g_0 + g_1) \cosh(g_1(y+Y)) - e^{-g_1 b}(g_0 - g_1) \cosh(g_1(y-Y))}{2g_0 g_1 \cosh(2g_1 b) + (g_0^2 + g_1^2) \sinh(2g_1 b)} ds \quad (4)$$

As in (1), the integration path follows the real s axis.

4. SECONDARY GREEN'S FUNCTION DERIVATION

In this section, the participant functions should be expressed in cylindrical coordinates with use of the well-known transformation relations: ($x = \rho \cos \phi$, $y = \rho \sin \phi$), ($X = P \cos \Phi$, $Y = P \sin \Phi$). Our purpose is to find the "secondary" Green's function, namely the field owed to the tiny metallic pin, through the scattering theorem employed in [21]. Consequently, we need the Green's function of the coupled cylinder-slab structure and the incident field upon it, developed by the singular source of the previous section. We note that both quantities refer to the system in the absence of the cylinder. The first one is the response of the device by an elementary dipole placed at the arbitrary position ($\rho = r$, $\phi = \gamma$) inside the slab (where the pin exists). The second one expresses the field produced by an identical dipole located along the axis ($\rho = P$, $\phi = \Phi$) equalling to $G_{1,sing}(\rho, \phi, P, \Phi) + G_{1,prim}(\rho, \phi, P, \Phi)$. As a result, one easily obtains the Green's function of the coupled structure by replacing (P, Φ) with (r, γ) in the previous formula. To this end, suppose that the developed

axial electric current on the PEC rod at $\rho = a$ equals to $K(\gamma, P, \Phi)$, $0 < \gamma < 2\pi$, where γ is the dummy azimuthal integration variable. In our case, the formula of the scattering integral is specialized to give:

$$G_{1,sec}(\rho, \phi, P, \Phi) = -jk_0\zeta_0a \int_0^{2\pi} [G_{1,sing}(\rho, \phi, a, \gamma) + G_{1,prim}(\rho, \phi, a, \gamma)] K(\gamma, P, \Phi) d\gamma \quad (5)$$

Due to the small size of the rod and its large distance from the strip, the current $K(\gamma, P, \Phi)$ can be approximated by an azimuthally invariant parameter, different for each combination of (P, Φ) , that is $K(\gamma, P, \Phi) \cong K(P, \Phi)$. Its value is determined by substituting (5) in the boundary condition for vanishing tangential (equaling total) electric field on the surface of the metallic scatterer $\rho = a$:

$$G_{1,sing}(a, \phi, P, \Phi) + G_{1,prim}(a, \phi, P, \Phi) + G_{1,sec}(a, \phi, P, \Phi) = 0 \quad (6)$$

and suppressing the ϕ -dependence via integration from 0 to 2π with respect to ϕ :

$$K(P, \Phi) = \frac{\int_0^{2\pi} [G_{1,sing}(a, \phi, P, \Phi) + G_{1,prim}(a, \phi, P, \Phi)] d\phi}{jk_0\zeta_0a \int_0^{2\pi} \int_0^{2\pi} [G_{1,sing}(a, \phi, a, \gamma) + G_{1,prim}(a, \phi, a, \gamma)] d\gamma d\phi} \quad (7)$$

The approximation described above contributes much in receiving the closed-form solution of the total problem.

By combining (5) and (7), a formula for the secondary Green's function is derived:

$$G_{1,sec}(\rho, \phi, P, \Phi) = - \int_0^{2\pi} [G_{1,sing}(\rho, \phi, a, \gamma) + G_{1,prim}(\rho, \phi, a, \gamma)] d\gamma \cdot \frac{\int_0^{2\pi} [G_{1,sing}(a, \phi, P, \Phi) + G_{1,prim}(a, \phi, P, \Phi)] d\phi}{\int_0^{2\pi} \int_0^{2\pi} [G_{1,sing}(a, \phi, a, \gamma) + G_{1,prim}(a, \phi, a, \gamma)] d\gamma d\phi} \quad (8)$$

The singular Green's function (free space term with wavenumber k_1) can be expanded to the following sum [22, p. 363]:

$$G_{1,sing}(\rho, \phi, \alpha, \beta) = -\frac{j}{4} \sum_{u=-\infty}^{+\infty} J_u(k_1 \min(\rho, \alpha)) H_u^{(2)}(k_1 \max(\rho, \alpha)) e^{-ju(\phi-\beta)} \quad (9)$$

where J_u is the Bessel function of u -th order. With use of (9), the integrations of (8) involving the singular component are analytically

carried out:

$$\int_0^{2\pi} G_{1,sing}(\rho, \phi, a, \gamma) d\gamma = -\frac{j\pi}{2} J_0(k_1 a) H_0^{(2)}(k_1 \rho) \quad (10)$$

$$\int_0^{2\pi} G_{1,sing}(a, \phi, P, \Phi) d\phi = -\frac{j\pi}{2} J_0(k_1 a) H_0^{(2)}(k_1 P) \quad (11)$$

$$\int_0^{2\pi} \int_0^{2\pi} G_{1,sing}(a, \phi, a, \gamma) d\gamma d\phi = -j\pi^2 J_0(k_1 a) H_0^{(2)}(k_1 a) \quad (12)$$

As far as the integrations of the primary part of the Green's function are concerned, the following alternative definitions for the Bessel function of zeroth order should be taken into account [22, p. 360]:

$$\int_0^{2\pi} e^{\pm\alpha(g_1 \sin \beta + j s \cos \beta)} d\beta = \int_0^{2\pi} e^{\pm\alpha(g_1 \sin \beta - j s \cos \beta)} d\beta = 2\pi J_0(k_1 \alpha) \quad (13)$$

Mind that the result is free of the spectral s parameter, a fact owing to our hypothesis for azimuthally independent surface current $K(P, \Phi)$. If one substitutes the harmonic and the hyperbolic functions in (4) by their exponential expressions and exploits (13), one concludes to the following simplified forms:

$$\int_0^{2\pi} G_{1,prim}(\rho, \phi, a, \gamma) d\gamma = J_0(k_1 a) \int_0^{+\infty} \frac{g_1 - g_0}{g_1} \cdot \frac{e^{-g_1 b} \cos(s\rho \cos \phi) \cosh(g_1 \rho \sin \phi)}{g_0 \cosh(g_1 b) + g_1 \sinh(g_1 b)} ds \quad (14)$$

$$\int_0^{2\pi} G_{1,prim}(a, \phi, P, \Phi) d\phi = J_0(k_1 a) \int_0^{+\infty} \frac{g_1 - g_0}{g_1} \cdot \frac{e^{-g_1 b} \cos(sP \cos \Phi) \cosh(g_1 P \sin \Phi)}{g_0 \cosh(g_1 b) + g_1 \sinh(g_1 b)} ds \quad (15)$$

$$\int_0^{2\pi} \int_0^{2\pi} G_{1,prim}(a, \phi, a, \gamma) d\gamma d\phi = J_0^2(k_1 a) \int_0^{+\infty} \frac{g_1 - g_0}{g_1} \cdot \frac{2\pi}{g_0 \cosh(g_1 b) + g_1 \sinh(g_1 b)} ds \quad (16)$$

The integration paths of the spectral integrals occupy now only the real positive semi axis as the functions $g_0(s), g_1(s)$ are even with respect to s .

By inspection of (14)–(16), one can notice that the integrands have the same branch points $s = k_0, k_1$ with the radiation functions $g_0(s), g_1(s)$ respectively [23]. By supposing that the shape of the

branch cuts does not change, we understand that all the integrand functions possess the branch cuts depicted in Fig. 2, which are lying exclusively on the lower half of the complex s plane for $\Re[s] > 0$. When it comes to the poles of these functions, they equal the zeros of the common denominator $\Pi(s)$:

$$\Pi(s) = \sqrt{s^2 - k_1^2} \cdot \left[\sqrt{s^2 - k_0^2} \cosh\left(b\sqrt{s^2 - k_1^2}\right) + \sqrt{s^2 - k_1^2} \sinh\left(b\sqrt{s^2 - k_1^2}\right) \right] \quad (17)$$

In case $s < k_0 < k_1$, the aforementioned function is nonzero because $\cosh^2(g_1 b) - \sinh^2(g_1 b) = 1$. In case $s > k_1$, the quantity is positive. Within the interval (k_0, k_1) , $\Pi(s)$ has at least one real root except for the trivial one at $s = k_1$. These roots correspond to the integrands' singularities which are integrable. Therefore, we are permitted to bypass them through a well-shaped path beginning at $s = k_0 - s_0$ and ending at $s = k_1 + s_1$ with $s_0, s_1 > 0$. As shown in Fig. 2, this path is lying on the upper half plane where the integrands are analytic.

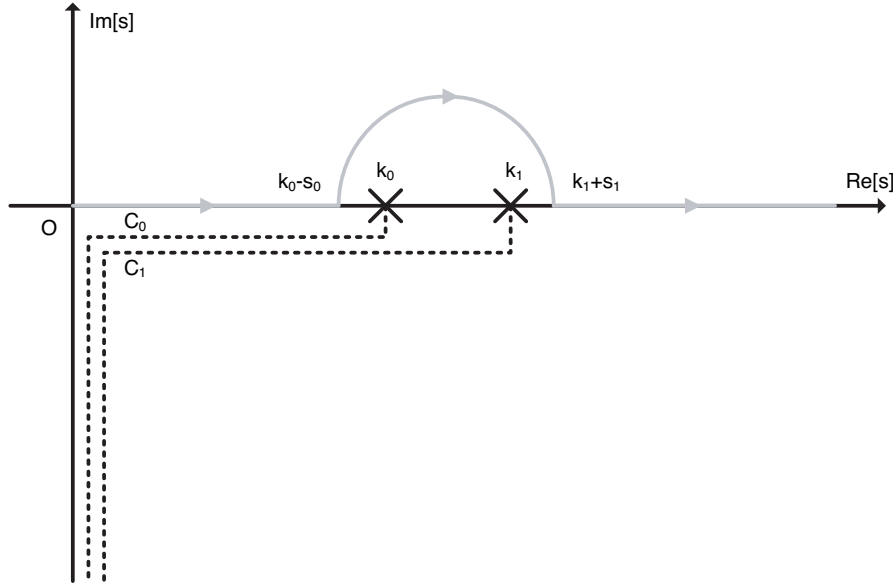


Figure 2. A presentation of the complex s spectral plane. The branch points $s = k_0, k_1$ of the integrands are marked by X and their branch cuts C_0, C_1 by dashed lines. The gray line represents the followed integration path which bypasses the singularities.

Due to the residue theorem, the value of the integral is not dependent on s_0, s_1 or the shape of the bypass.

5. INTEGRATION ALONG THE STRIP

A prerequisite to proceed in the computation of the total electric field is the polar equation of the strip. The carrier line's equation on the $x - y$ plane is written as: $y = (x + D) \tan \theta$. Through the transformation formulas ($x = R \cos F, y = R \sin F$), we retrieve the following polar expression $R(F)$:

$$R(F) = \frac{D \tan \theta}{\sin F - \cos F \tan \theta}, \quad F_1 < F < F_2 \quad (18)$$

where F_1, F_2 are the angles defining the extent of the strip presented in Fig. 3. With reference to it, we apply the law of cosines to the triangles (OMP_1) and (OMP_2) to determine their unspecified sides. In particular, we obtain $(OP_1) = \sqrt{D^2 + h^2 - 2Dh \cos \theta}$ and $(OP_2) = \sqrt{D^2 + h^2 + 2Dh \cos \theta}$. By utilizing the law of sines to each triangle, the following values for F_1, F_2 are received:

$$F_1 = \pi - \arcsin \left(\frac{h \sin \theta}{\sqrt{D^2 + h^2 - 2Dh \cos \theta}} \right) \quad (19)$$

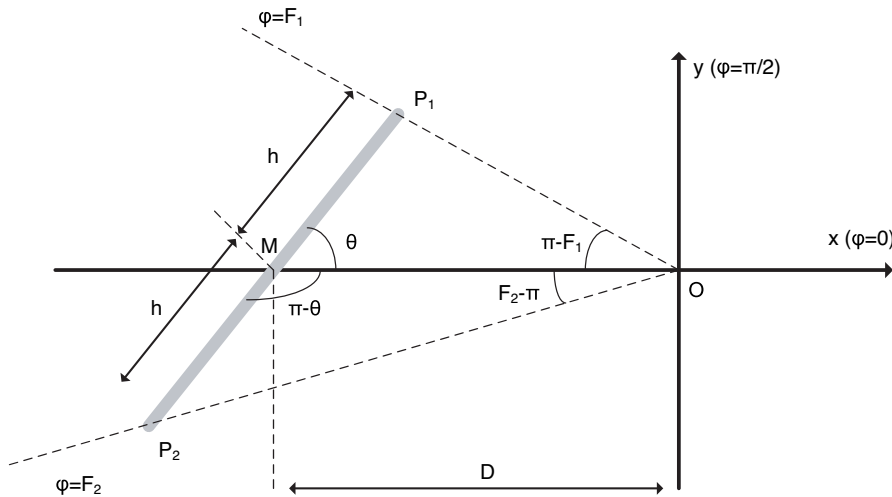


Figure 3. The geometric triangle formed by the origin O and the ends of the strip P_1, P_2 . The angles defining the extent of the source are denoted by F_1, F_2 .

$$F_2 = \pi + \arcsin\left(\frac{h \sin \theta}{\sqrt{D^2 + h^2 + 2Dh \cos \theta}}\right) \quad (20)$$

with $\arcsin(z) \in (-\pi/2, \pi/2)$.

The scattering integral will appear again in manipulating the strip excitation. The total axial electric field inside the slab is given by:

$$E_{z1}(x, y) = -jk_0\zeta_0 I \int_{F_1}^{F_2} G_1(x, y, R(F), F) \sqrt{R^2(F) + R'^2(F)} dF \quad (21)$$

where G_1 is the total Green's function for observation points inside the dielectric waveguide:

$$G_1(x, y, P, F) = G_{1,sing}(x, y, P, F) + G_{1,prim}(x, y, P, F) + G_{1,sec}(x, y, P, F) \quad (22)$$

The quantity multiplying the Green's function in (21), is necessary for the evaluation of a line integral [15]. In our case, it is simplified to give:

$$\sqrt{R^2(F) + R'^2(F)} = \frac{D \sin \theta}{\sin^2(\theta - F)} \quad (23)$$

6. NUMERICAL RESULTS

6.1. Presentation of Output and Input Parameters

A set of computer programs has been developed for the calculation of certain quantities describing the operation of the device. The magnitude of the total electric field $|E_{z1}(x, y)|$ is evaluated through (21) and expresses the distribution of the electromagnetic energy in two or one dimension (for constant x) inside the slab. The current $K(P, \Phi)$ around the pin is specified by (7). However, we introduce a modified parameter κ to take into account the excitation from the whole strip:

$$\kappa = \left| \int_{F_1}^{F_2} K(R(F), F) \sqrt{R^2(F) + R'^2(F)} dF \right| \quad (24)$$

The line integral κ is called "total cylinder current" expressed in A. Another interesting variable will be the propagated power within the slab given by:

$$\sigma(x) = \frac{k_1}{k_0\zeta_0} \int_{-b}^b |E_{z1}(x, y)|^2 dy \quad (25)$$

It is defined with respect to the wavenumber $s = k_1$ which is close to the (always supported and guided) fundamental mode.

When it comes to the input parameters, they should possess certain values serving the demands of optical waveguide applications. The typical value for the operating frequency is very high: $f = 300$ THz and varies within the interval: $(100, 500)$ THz. The relative permittivity of the slab's silicon-type material is slightly larger than unity: $\epsilon_1 \in (1.01, 2)$ and usually taken equal to 1.5. The thickness of the slab belongs in $(0.5, 2.5) \mu\text{m}$ so that only few modes will propagate (typical value: $b = 1.5 \mu\text{m}$) [24]. The length of the strip is basically picked from the continuous set: $(b/20, b/2)$, while it equals to: $h = b/4$ for fixed- h applications. In addition, the usual position of the strip is the vertical one: $\theta = \pi/2$, even though there is no constraint in the value of the angle expressing the bevel of the strip: $\theta \in (0, \pi)$. The excitation source is centralized at a fixed point: $D = 5 \mu\text{m}$ and we commonly investigate the region of the slab with: $x \in (2, 6) \mu\text{m}$ (typical value: $x = 4 \mu\text{m}$). The radius of the cylinder is tiny and invariant throughout the simulations: $a = 0.005 \mu\text{m}$, whereas the magnitude of the excitation current is kept constant: $I = 0.001$ A/m.

6.2. Approximate Evaluation of the Integrals

A major part of the computations producing the variation graphs of the output quantities is the numerical integrations on the spectral complex plane (4), (7), (14)–(16) and across the strip's line (21). The spectral integrals are of infinite interval and therefore the asymptotic forms for the corresponding integrand functions as $s \rightarrow +\infty$ should be extracted. In particular, the integrands of (14), (15) behave like $O[\exp(s(|Y| - 2b)/s)]$, $s \rightarrow +\infty$. The integrand of (16) follows the law $O[\exp(-sb)/s]$, $s \rightarrow +\infty$, while the one of (4) varies as $O[\exp(s(|Y + y| - 2b))/s]$, $s \rightarrow +\infty$ for large positive arguments. These expansions help us in deciding a suitable truncation upper limit s_{max} . In all the examined cases, a choice $s_{max} = 5k_0$ is appropriate, even when the ends of the strips are relatively close to the horizontal bounds and the observation points upon these separating planes.

As far as the parameters s_0, s_1 are concerned, they are chosen equal to each other and relatively small compared to k_0 , otherwise numerical problems are occurred. That is because the bypass has semicircular shape with radius $(k_0 + k_1)/2 + s_0 = (k_0 + k_1)/2 + s_1$ and the imaginary parts of some of the circumvention points are large. It should be pointed out that we checked if the value of each integral remains exactly the same for different $s_0 = s_1$. Another issue relating to the spectral integrations is the harmonic factor of the integrands which is oscillating rapidly when the observation point gets horizontally

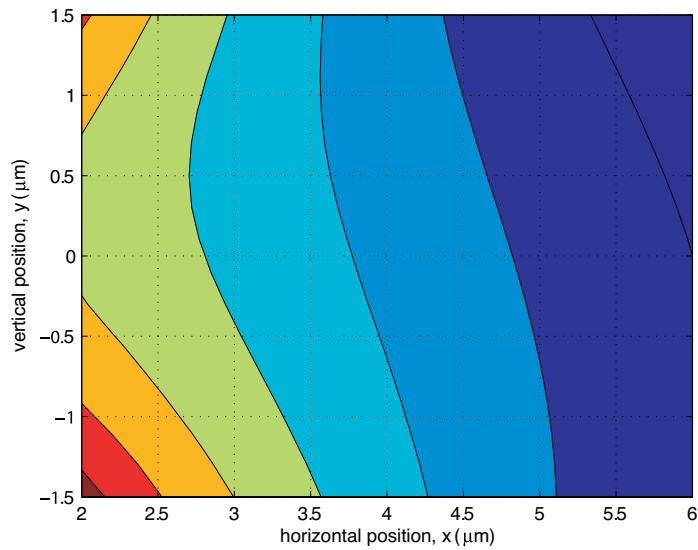
distant from the source. In our applications this is not the case because x is moderate. To compute the integrals we used the trapezoidal rule with $s_{ppw} = 200$ points per wavelength λ_0 of s_{max} leading to convergent results for all the investigated cases. The line integrations with respect to F are carried out more easily because the interval is finite and the integrands are smooth. That is because θ couples to angles F_1, F_2 between which the denominator $\sin^2(\theta - F)$ is nonzero. Thus, a straightforward trapezoidal integration with $F_{ppw} = 100$ points per wavelength λ_0 of the strip's length is sufficient to ensure reliable results.

6.3. Numerical Simulations and Discussion

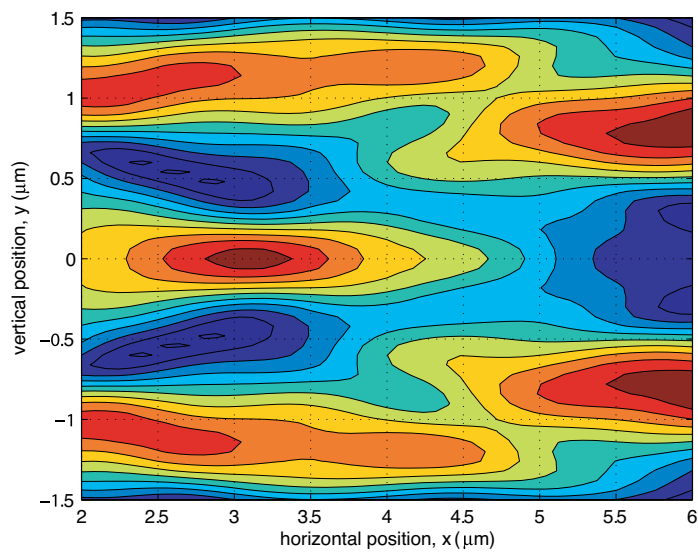
In Figs. 4 we present the variation of the electric field's magnitude in two dimensions inside the slab. In Fig. 4(a) the operating frequency is small ($f = 100$ THz) and the dielectric owns a low permittivity $\epsilon_1 = 1.01$. One can observe the weaker field close to the upper separating plane $y = b$ compared to the lower one's because of the skew position of the strip $\theta = \pi/4$. In addition, the fluctuation of the quantity with respect to y variable decreases with increasing x distance from the source. In Fig. 4(b) we examine an optically denser material with $\epsilon_1 = 2$ excited at higher frequencies $f=500$ THz. The spatial oscillations towards both directions are more rapid due to the large value of k_1 and the contour plot is symmetric with respect to $y = 0$, reflecting the symmetry of a structure with vertical strip ($\theta = \pi/2$).

In Figs. 5 we show the variation of $|E_{z1}(x, y)|$ (for fixed $x = 4 \mu\text{m}$) with respect to $y \in (-b, b)$, for three different inclinations θ . In Fig. 5(a) the length of the strip is small: $h = b/20$ and thus all the curves are almost identical. In the limit $h \rightarrow 0$, the excitation is independent from θ . Three maxima of the field are recorded along the cross section of the slab, one of which at $y = 0$, while the shapes are quasi-symmetrical with respect to it. In Fig. 5(b) we choose a lengthy source with $h = b/2$ and therefore the values of the field are significantly increased compared to Fig. 5(a). Once more, the curve corresponding to $\theta = \pi/2$ is symmetric, while the other two curves obey the property of a flip symmetry. The face of the strip is directed to the side of more substantial magnitudes. It is also notable that the curves of $\theta = \pi/4, 3\pi/4$ vanish close to $y = \pm 1 \mu\text{m}$ respectively.

In Fig. 6(a) are represented graphs of total cylinder current κ as function of h/b (with fixed $b = 4 \mu\text{m}$) for several θ . With increasing θ (kept below $\pi/2$) the current on the pin gets more substantial. This is attributed to the greater effect of the excitation on the system. When h/b is vanishing, the three curves coincide each other for reasons explained above. It is noteworthy that the current is heavily dependent

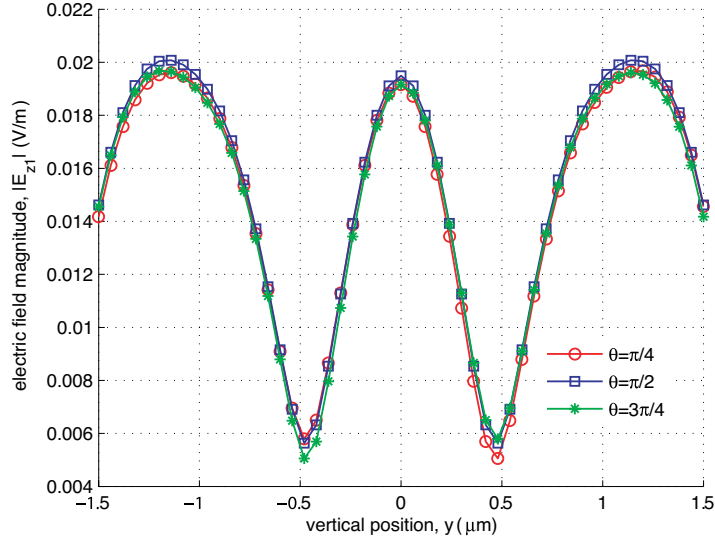


(a)

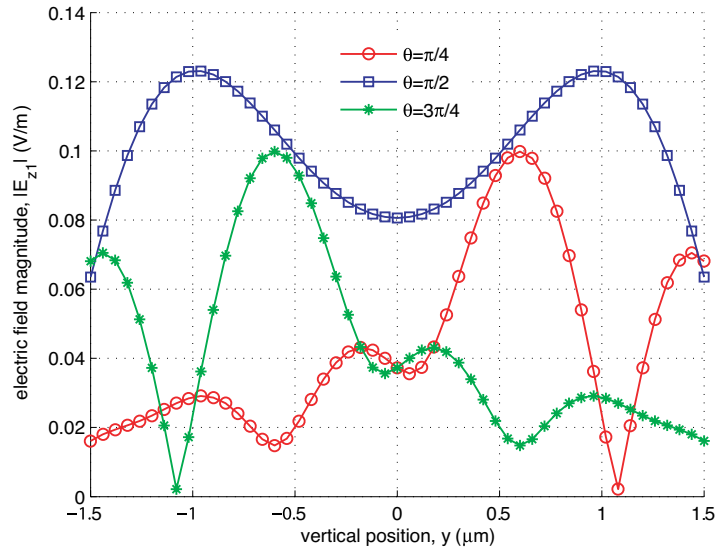


(b)

Figure 4. The contour plot of the electric field's magnitude inside the slab. (a) $f = 100$ THz, $\epsilon_1 = 1.01$, $\theta = \pi/4$, (b) $f = 500$ THz, $\epsilon_1 = 2$, $\theta = \pi/2$. Other parameters: $b=1.5 \mu\text{m}$, $h = b/4$, $a = 0.005 \mu\text{m}$, $I = 0.001$ A, $D = 5 \mu\text{m}$.



(a)



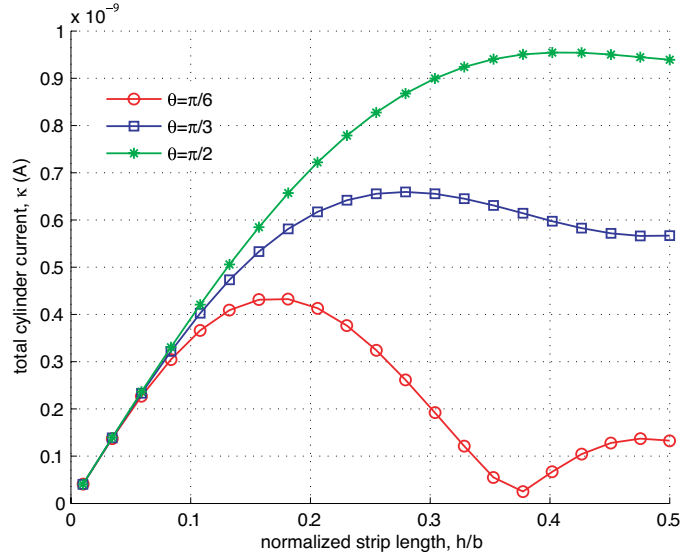
(b)

Figure 5. Magnitude of electric field as function of vertical distance for various strip angles. (a) $h=b/20$, (b) $h = b/2$. Other parameters: $f = 300$ THz, $\epsilon_1 = 1.5$, $b = 1.5 \mu\text{m}$, $a = 0.005 \mu\text{m}$, $I = 0.001$ A, $D = 5 \mu\text{m}$, $x = 4 \mu\text{m}$.

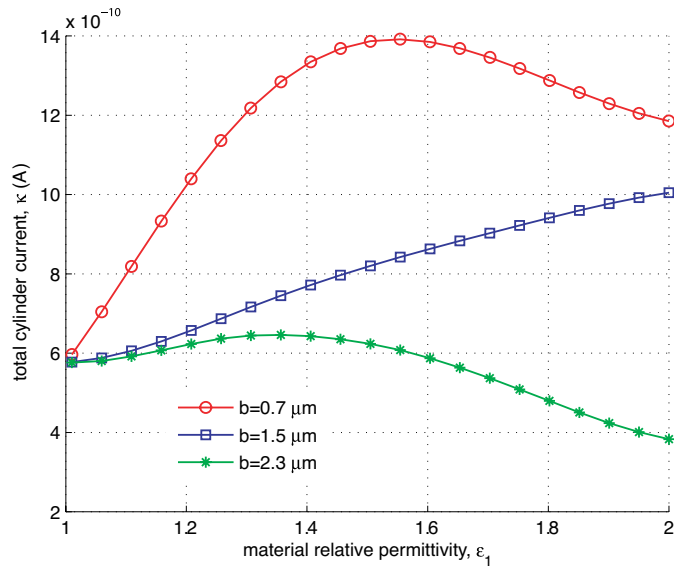
on h/b for smaller θ . That is because the minimum distance between the cylinder and the strip varies to greater extent when θ takes lower values. In Fig. 6(b) are represented graphs of κ as function of ϵ_1 (with fixed $h = 0.375 \mu\text{m}$) for various b . At the leftmost point of the diagram, namely when $\epsilon_1 \rightarrow 1$, all the curves concur. This is sensible as the material of the slab is vacuum in this case, and thus the thickness b plays no role. In addition, the pin's current is reinforced with decreasing b due to the significant concentration of energy into the slab and around the scatterer. It is also noticed that the curve for $b = 2.3 \mu\text{m}$ is decaying with respect to ϵ_1 , contrary to the one of $b = 1.5 \mu\text{m}$ which is upward sloping and the third one which is oscillating.

In Figs. 7 we depict the propagated power $\sigma(x)$ for constant $x = 4 \mu\text{m}$ as function of θ for four different ratios h/b . In Fig. 7(a) the slab's thickness is chosen relatively small: $b = 0.5 \mu\text{m}$ and the waveguide's material almost vacuum: $\epsilon_1 = 1.01$. The increasing length of the strip makes naturally the excitation source more powerful and thus the energy is proportional to h . A maximum is observed at $\theta = \pi/2$ for all the symmetric curves which becomes less apparent for decreasing h/b . In other words, the influence of the source is maximized at $\theta = \pi/2$, where it is strongly affected by the extent of the strip. In Fig. 7(b) both the slab's thickness and the permittivity are picked with large magnitudes: $b = 2.5 \mu\text{m}$, $\epsilon_1 = 2$. The power levels are higher than in Fig. 7(a) since the greater permittivity of the material increases the power within the waveguide. Furthermore, the impact of the strip gets almost negligible for $\theta \rightarrow 0, \pi$ and suddenly increases at $\theta \cong 0.7$. With the exception of the case corresponding to $h/b = 1/8$, the maximum value is not single and is not exhibited at $\theta = \pi/2$ this time. For the curves with: ($h/b = 1/4, 3/8, 1/2$) two maxima, getting sharper as h/b increases, are observed at symmetric positions with respect to $\theta = \pi/2$.

In Figs. 8 we present the propagated power $\sigma(x)$ as function of the slab's thickness for various material permittivities with fixed $x = 4 \mu\text{m}$. In Fig. 8(a) we select a low inclination of the strip's line $\theta = \pi/10$ for which all the curves are oscillating and (on average) increasing. That is because more spatial fluctuations are carried out and more energy is channeled into the device for higher b . Furthermore, the variation is more substantial for small b as in these cases the ends of the strip are close to the separating planes $y = \pm b$. In Fig. 8(b) the strip is vertical ($\theta = \pi/2$) and therefore the magnitudes of the power are amplified. Moreover, the curves for $\epsilon_1 = 1.5, 1.7, 1.9$ seem to have a common nonzero limit for large b . On the contrary, the curve corresponding to $\epsilon_1 = 1.3$ is decaying since the permittivity is too low to gather much power into the waveguide.

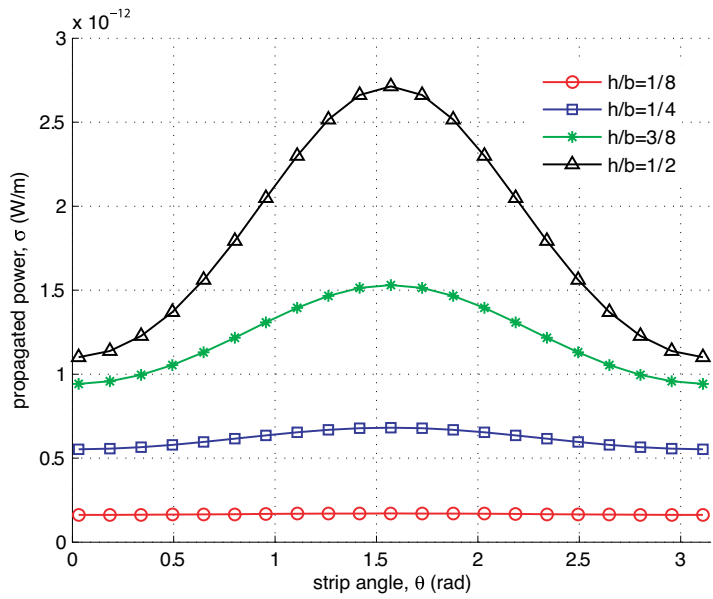


(a)

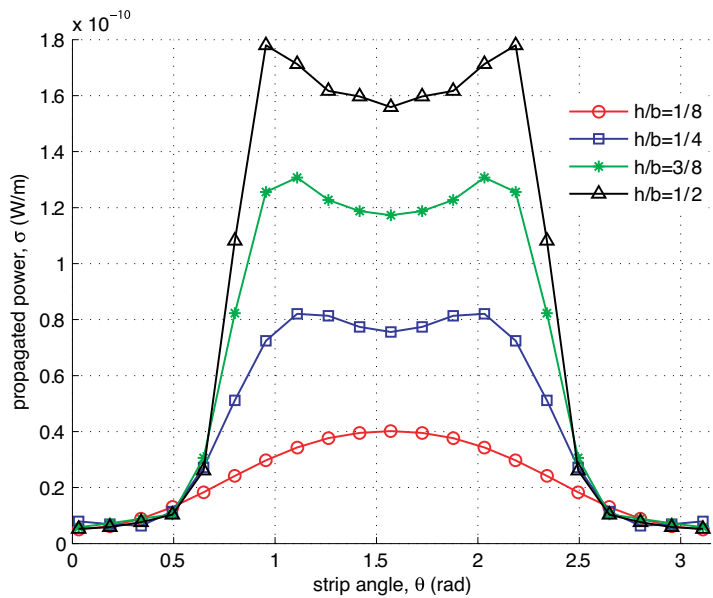


(b)

Figure 6. Total cylinder current (a) as function of the normalized strip length for various line inclinations with $\epsilon_1 = 1.5$, $b = 1.5 \mu\text{m}$, (b) as function of the material relative permittivity for various slab thicknesses with $\theta = \pi/2$, $h = 0.375 \mu\text{m}$. Other parameters: $f = 300 \text{ THz}$, $a = 0.005 \mu\text{m}$, $I = 0.001 \text{ A}$, $D = 5 \mu\text{m}$, $x = 4 \mu\text{m}$.

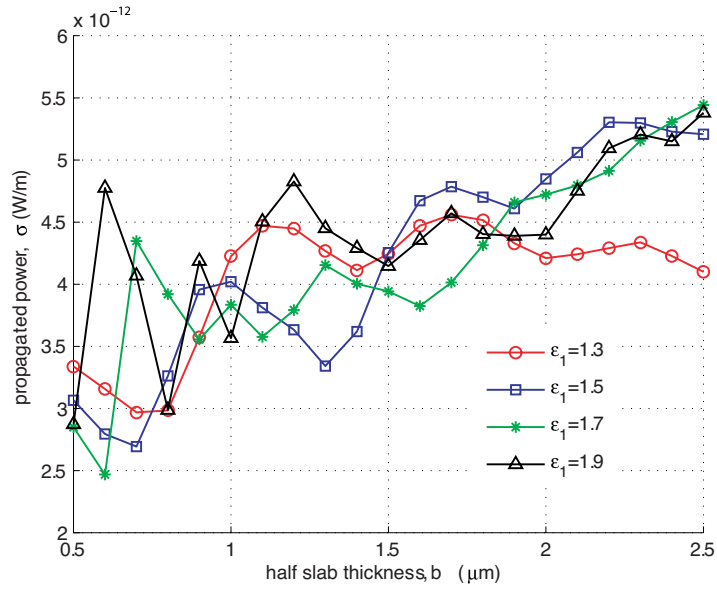


(a)

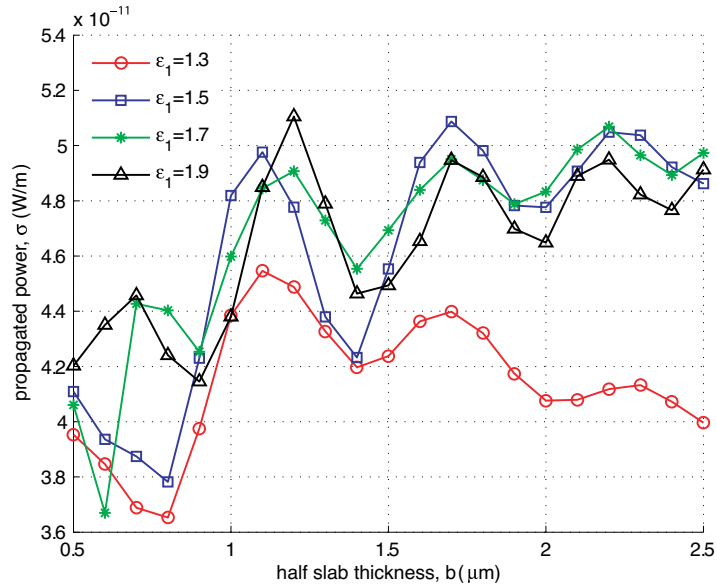


(b)

Figure 7. The propagated power as function of the strip's angle for various lengths. (a) $\epsilon_1 = 1.01$, $b = 0.5 \mu\text{m}$, (b) $\epsilon_1 = 2$, $b = 2.5 \mu\text{m}$. Other parameters: $f = 300 \text{ THz}$, $a = 0.005 \mu\text{m}$, $I = 0.001 \text{ A}$, $D = 5 \mu\text{m}$, $x = 4 \mu\text{m}$.



(a)



(b)

Figure 8. The propagated power as function of the slab's thickness for various permittivities. (a) $\theta = \pi/10$, (b) $\theta = \pi/2$. Other parameters: $f = 300$ THz, $h = 0.375 \mu\text{m}$, $a = 0.005 \mu\text{m}$, $I = 0.001$ A, $D = 5 \mu\text{m}$, $x = 4 \mu\text{m}$.

7. CONCLUSION

A dielectric waveguide with an embedded metallic pin is excited by a skew strip flown by constant current. Due to the small size of the conducting scatterer, a closed-form solution to the described problem can be found. A polar form of the strip's line is necessary for the evaluation of the scattering integral. Numerous graphs of the electric field into the slab, the surface current on the pin and the propagated power are presented and discussed.

Similar techniques can be employed to treat a slab problem with multiple metallic pins inside it. Each of the cylinders could be of constant current independent from the others due to the infinitesimal size. Optimization problems with respect to the positions of the pins may be obtained for various application-defined objectives. The case of coupled waveguides and the role played by the skew source line to the interaction of the slabs is also worth to be examined. Finally, excitation strips of arbitrary shape and their effect to the device's features could be an interesting issue for further investigation.

REFERENCES

1. Balanis, C. A., *Advanced Engineering Electromagnetics*, 414–431, John Wiley & Sons, New York, 1989.
2. Mohsen, A. A., E. M. A. Elkaramany, and F. G. A. El-Hadeed, “Two dimensional long transmission line-frequency domain (LTL-FD) treatment of dielectric loaded waveguides,” *Journal of Electromagnetic Waves and Applications*, Vol. 15, No. 7, 901–911, 2001.
3. Kobayashi, K., S. Koshikawa, and A. Sawai, “Diffraction by a parallel-plate waveguide cavity with dielectric/ferrite loading: Part I — the case of E polarization,” *Progress In Electromagnetics Research*, PIER 8, 377–426, 1994.
4. Attiya, A. M., A. A. Kishk, and A. W. Glisson, “Analysis of two-dimensional magneto-dielectric slab,” *Progress In Electromagnetics Research*, PIER 74, 195–216, 2007.
5. Chang, H.-W. and W.-C. Cheng, “Analysis of dielectric waveguide termination with tilted facets by analytic continuity method,” *Journal of Electromagnetic Waves and Applications*, Vol. 21, No. 12, 1621–1630, 2007.
6. Liu, S.-H., C.-H. Liang, W. Ding, L. Chen, and W.-T. Pan, “Electromagnetic wave propagation through a slab waveguide

- of uniaxially anisotropic dispersive metamaterial,” *Progress In Electromagnetics Research*, PIER 76, 467–475, 2007.
7. Lu, J., B.-I. Wu, J.-A. Kong, and M. Chen, “Guided modes with a linearly varying transverse field inside a left-handed dielectric slab,” *Journal of Electromagnetic Waves and Applications*, Vol. 20, No. 5, 689–697, 2006.
 8. Attiya, A. M. and A. A. Kishk, “Modal analysis of a two-dimensional dielectric grating slab excited by an obliquely incident plane wave,” *Progress In Electromagnetics Research*, PIER 60, 221–243, 2006.
 9. Kalinichev, V. I. and N. M. Solovev, “Modal diffraction of dielectric-slab surface waves by a metallic cylinder,” *Radiotekhnika i Elektronika*, Vol. 35, No. 2, 241–251, 1990.
 10. Terracher, F. and G. Berginc, “A numerical study of TM-type surface waves on a grounded dielectric slab covered by a doubly periodic array of metallic patches,” *Progress In Electromagnetics Research*, PIER 43, 75–100, 2003.
 11. Leung, K. W. and H. K. Ng, “Theory and experiment of circularly polarized dielectric resonator antenna with a parasitic patch,” *IEEE Transactions on Antennas and Propagation*, Vol. 51, No. 3, 405–412, 2003.
 12. Cooray, F. R. and J. S. Kot, “Analysis of radiation from a cylindrical-rectangular microstrip patch antenna loaded with a supersrate and an air gap, using the electric surface current model,” *Progress In Electromagnetics Research*, PIER 67, 135–152, 2007.
 13. Liu, Z., M. He, and H. Xiong, “The design of a sensor with flexible circuit excitation in electromagnetic tomography system,” *Journal of Physics: Conference Series*, Vol. 15, 276–281, 2005.
 14. Cuthbert, M. A., A. Z. Elsherbeni, C. E. Smith, C. W. P. Huang, and K. F. Lee, “Tapered meander slot antenna or dual band personal wireless communication systems,” *Microwave and Optical Technology Letters*, Vol. 36, No. 5, 381–385, 2003.
 15. Valagiannopoulos, C. A., “Study of an electrically anisotropic cylinder excited magnetically by a straight strip line,” *Progress In Electromagnetics Research*, PIER 73, 297–325, 2007.
 16. Geran, F., G. Dadashzadeh, M. Fardis, N. Hojjat, and A. Ahmadi, “Rectangular slot with a novel triangle ring microstrip feed for UWB applications,” *Journal of Electromagnetic Waves and Applications*, Vol. 21, No. 3, 387–396, 2007.

17. Rezaei, F. P., M. Hakkak, and K. Forooraghi, "Effect of magnetic layer on the microstrip-excited rectangular dielectric resonator antennas bandwidth," *Journal of Electromagnetic Waves and Applications*, Vol. 21, No. 7, 915–927, 2007.
18. Valagiannopoulos, C. A., "Effect of cylindrical scatterer with arbitrary curvature on the features of a metamaterial slab antenna," *Progress In Electromagnetics Research*, PIER 71, 59–83, 2007.
19. Valagiannopoulos, C. A., "Arbitrary currents on circular cylinder with inhomogeneous cladding and RCS optimization," *Journal of Electromagnetic Waves and Applications*, Vol. 21, No. 5, 665–680, 2007.
20. Duffy, D., *Green's Functions with Applications*, 280–285, CRC Press, New York, 2001.
21. Valagiannopoulos, C. A., "Single-series solution to the radiation of loop antenna in the presence of a conducting sphere," *Progress In Electromagnetics Research*, PIER 71, 277–294, 2007.
22. Abramowitz, M. and I. Stegun, *Handbook of Mathematical Functions*, National Bureau of Standards, Washington, 1970.
23. Schevchenko, V., *Continuous Transitions in Open Waveguides*, 24–26, Golem, 1971.
24. Christian, N. L. and L. K. Passauer, *Fiber Optic Component Design, Fabrication, Testing, Operation, Reliability, and Maintainability*, 62–65, Noyes Data, New Jersey, 1989.